Int. J. Heat Mass Transfer. Vol. 22, pp. 1165–1174
Pergamon Press Ltd. 1979. Printed in Great Britain

NON-DARCY FLOW WITH CHANGE OF PHASE IN INTERNALLY ENERGISED FLAT SHAPED POROUS ELEMENT

DAVID MOALEM MARON and SHIMON COHEN
Department of Fluid Mechanics and Heat Transfer, School of Engineering,
Tel-Aviv University, Israel

(*Received* 25 *April* 1977 *and in revised form* 21 *June* 1977)

Abstract—A theoretical analysis of fluid flow through internally heated porous medium under phase conversion and vapour superheat is presented. Non-Darcy flow regime is considered. The temperature distributions in the solid and fluid phases are solved simultaneously and the difference between the two in steady operation is found to be relatively small. Characteristic parameters for various operational conditions are evaluated and computed, including the rate of internal heat generation required.

NOMENCLATURE

A, dimensionless group $\left(=\frac{a}{a_g}\frac{v_f}{v_l}\right)$;

a, viscous coefficient;

B, dimensionless group $\left(=Re\frac{\rho_l}{\rho_f}\frac{b}{b_g}\right)$;

b, inertial coefficient;

C_0, C_1, C_3, C_4, constants of integration;

C_{pf}, specific heat;

$C_{pl,v}$, liquid to vapour specific heat ratio (C_{pl}/C_{pv});

D_p, particle diameter;

D_f dimensionless group $\left(=\frac{C_{pf}\dot{m}_f(r_0-r_i)^{1-n}}{(2\pi)^n k_f \varepsilon}\right)$;

Ja, Jakob number $(=\lambda\rho_v/C_{pl}\rho_l(T_0-T_i)$;

k, thermal conductivity;

$K_{s,f}$ solid to fluid thermal conductivity ratio $[=k_s(1-\varepsilon)/(\varepsilon k)]$;

l, characteristic length $(=b/a)$;

$\dot{m}_f$, mass flow rate;

$\dot{M}_f$, dimensionless mass flow rate $[=\dot{m}_f/(\rho_l\bar{v}(r_0-r_i)^n]$;

$\dot{M}$, dimensionless flow rate, $M=\dot{M}_n=\dot{M}_l=\dot{M}_v$;

N, dimensionless rate of heat generation $\left[=\frac{q(r_0-r_i)^2}{(T_0-T_i)k_s(1-\varepsilon)}\right]$;

Nu_s, Nu_f, Nusselt number in the solid and fluid phase, respectively;

$Nu_{s,f}$, solid to fluid Nusselt number ratio $(=Nu_s/Nu_f)$;

p, pressure;

P, dimensionless pressure $\left(=\frac{p-p_0}{p_i-p_0}\right)$;

q, rate of volumetric heat generation;

q_r, rate of heat flux;

Q_r, dimensionless heat flux rate $\left[=\frac{q_r(r_i-r_0)}{(T_0-T_i)k_l\varepsilon}\right]$;

r, axial coordinate;

R, dimensionless axial coordinate $[=r/(r_0-r_i)]$;

Re, Reynolds number $\left(=\frac{\bar{v}}{v_{,l}}\frac{b_g}{a_g}\right)$;

T, temperature;

$\bar{v}$, overall average Darcy-velocity $\left(=-\frac{\kappa}{\mu_l}\frac{p_i-p_0}{r_i-r_0}\right)$;

v_r, axial velocity;

V_r, dimensionless velocity $(=v_r/\bar{v})$.

Greek symbols

α, β, γ, roots of the cubic equation in equation (16);

ε, porosity;

ρ, density;

$\rho_{l,v}$, liquid to vapour density ratio $(=\rho_l/\rho_v)$;

κ, permeability of porous structure;

λ, latent heat of vapourization;

θ, dimensionless temperature $[=(T-T_i)/(T_0-T_i)]$;

μ, viscosity;

ν, kinematic viscosity $(=\mu/\rho)$;

$\nu_{l,v}$, liquid to vapour kinematic viscosity ratio $(=\nu_l/\nu_v)$.

Subscripts

b, end of dispenser domain;

c, start of evaporation regime;

d, end of saturation regime;

f, fluid (liquid or vapour);

g, heater porous phase;

l, liquid;

i, reservoir;

n, liquid in dispenser domain;

r, radial;

s, solid;

t, total;

v, vapour;

w, entry side of dispenser;
*, saturation state (superscript);
0, external side of slab or cylinder.

(A) INTRODUCTION

RECENT interest in convective two-phase heat transfer in porous media arises from its extensive and common occurrence in many engineering applications and due to its particular relevance to various practical fields. A wide range of related problems is described by Moalem [1] and the corresponding references are also classified and named [2].

Of a considerable interest is the problem associated with combined heat and mass transfer in internally energised porous medium. The principle of internal heat generation within saturated porous matrix may prove useful, particularly where specific powers are relatively high, in which case the use of working surface is unsuitable due to poor heat-transfer characteristics. High heat absorbing capacity of a coolant may be achieved under phase-conversion and vapor superheat. Moreover, the enormous specific surface of porous reactors enables high specific ratings even with small temperature driving forces between the energised solid and the working fluid.

A steady state solution of the heat-transfer rates in porous media with temperature-dependent internal energy source has been recently presented by Moalem [1, 2]. The concept of generating internal heat of a temperature dependent rate seems to be promising in concern to stability of operation and long life element due to the dynamic self control, which such an element possesses.

An attempt to evaluate the heat-transfer characteristics of internally heated porous element in transient operation has been recently reported by Moalem and Cohen [3]. The steady state solutions [1,2] yield the variation of the required internal heat load of the element and the corresponding mass flow rate of the working fluid with the degree of superheat at the exit surface. The study into the transient part of the problem is aimed at the understanding of the reactor performance on start-up and shut-down. Both the steady and transient studies, consider a representative range of the viscous flow regime, in which case the heterogeneous solid–fluid system is treated as a continuum. Hence, average or "macroscopic" governing equations can be reasonably applied. The assumption of equal temperatures of the solid and the adjacent fluid is consistent with slow flows through the porous medium, [4, 5].

The overall heat-transfer performance may be further improved by resorting to high fluid velocities through the solid matrix. However, in contrast to the voluminous research done on slow flows, rapid flow through porous materials has received comparatively little attention until recently [6].

The present study deals with the phenomenon of fluid flow through internally heated porous medium, and constitutes an attempt to extend the previous works [1, 2] to non-Darcy flow regimes. Constant rate of heat generation is assumed where the solid particles forming the porous structure may be nuclear or electrically heated. Heat may be generated also due to the absorption of radiation. The fluid passed through the heated porous medium may change from liquid to vapor and the vapor be further superheated.

In a fluid–solid porous reactor element an operational instability can result at high temperature due to both the relationship between fluid viscosity and temperature and the non-uniformity of the fluid flow in the porous structure. This instability problem can be avoided if a dual layer material in the heating regime is used [7, 8]. The inner layer (Disperser) is of a relatively low permeability while the outer layer is of a high thermal conductivity and a high permeability. The effect of the dispenser layer is also accounted for in the present analysis.

(B) THE THEORETICAL MODEL AND GOVERNING EQUATIONS

Typical porous elements of different geometry are sketched in Fig. 1(a) and 1(b). The former represents an internally energised porous slab of thickness L $(=R_0-R_i)$ while the latter is in the form of a hollow porous cylinder, where the flow may be from either the inside or the outside. Here, the liquid is assumed

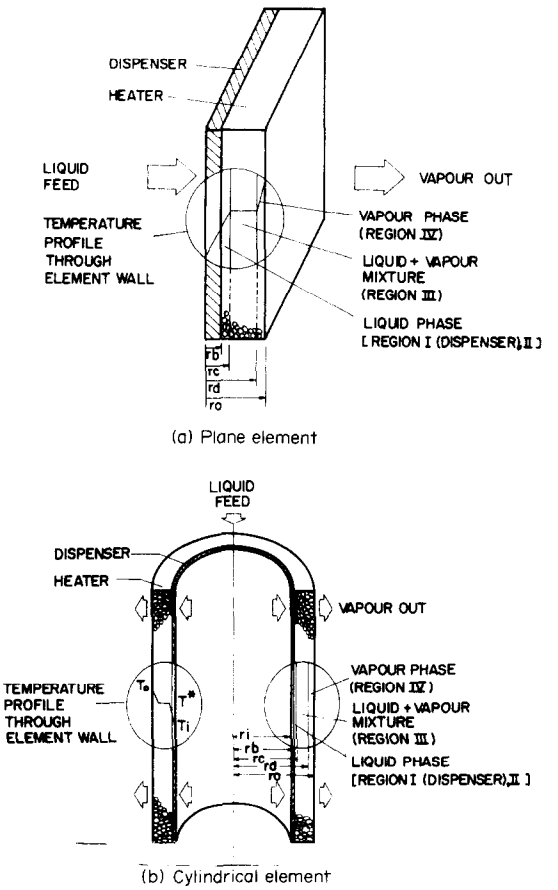

FIG. 1. Schematic presentation of a dual-layer porous reactor.

to flow radially outwards through the porous medium by an imposed total pressure drop of $p_i - p_0$, where p_i and p_0 are the pressures maintained at the rear surface upstream and at the leading surface downstream, respectively. Note that in each case the dispenser is placed upstream as is shown in Fig. 1.

In the pressure gradient considered here, the equation of motion is given by the modified Darcy's law as was shown by Green and Duwez [9]:

$$-\frac{dp}{dr} = a\mu_f v_r + b\rho_f v_r^2 \tag{1}$$

where the constants $a(=1/\kappa)$ and b are the viscous and the inertial coefficients, respectively and are determined by the properties of the porous material only and depend neither on the type of fluid nor on the material temperature [10]. κ is the permeability of the porous structure and dp/dr is the radial pressure gradient which corresponds to a radial valocity v_r of a single-phase fluid of density ρ_f and viscosity μ_f. Note that, as the coolant approaches the inlet surface, the pressure drop from flow acceleration is small compared with the drop through the porous material so that $p_i \sim p_\infty$, where p_∞ being the reservoir pressure. Neglecting the transient term the equation of continuity may be written in general form:

$$\frac{d}{dr}(\rho_f r^n v_r) = 0 \quad n = \begin{cases} 0\text{—plane} \\ 1\text{—cylindrical} \end{cases} \tag{2a}$$

where v_r is the radial superficial velocity and ρ_f is the fluid density. In the case of steady-state operation, equation (2a) may simply be reduced to:

$$\rho_f r^n v_r = \text{Constant} = \frac{\dot{m}_f}{(2\pi)^n} \tag{2b}$$

where $\dot{m}_f$ is either the mass flux in the case of plane configuration ($n = 0$), or the mass flow rate per unit length of cylinder ($n = 1$). *Utilizing equation* (2*b*), *equation* (1) *may now be written in the form:*

$$-\frac{dp}{dr} = \frac{a v_f \dot{m}_f}{(2\pi)^n}\frac{1}{r^n} + \frac{b\dot{m}_f^2}{(2\pi)^{2n}\rho_f}\frac{1}{r^{2n}} \tag{2c}$$

Energy is generated in the medium at an arbitrary volumetric rate q. After a time-interval the temperature at the outlet side reaches the boiling point of the liquid, and evaporation may take place within the medium. If the rate of heat generation is large enough the liquid feed is completely converted to saturated vapor and the saturated vapor is further superheated until steady-state is reached. It is assumed that at steady-state operation the regions of different phases are "seperated" by two phase-change "interfaces", the first of which (at r_c) denotes the average distance where evaporation starts and the second (at r_d) denotes the average distance where complete evaporation is reached. The liquid passed through the heated porous medium, is firstly heated to saturation state in region I, changes phase from liquid to vapor in region II, and the vapor is further superheated in region III to an exit temperature T_0, greater than the saturation temperature of the liquid corresponding to the pressure p_0. The temperature and pressure at the evaporation region are the saturation temperature and pressure T^* and p^*, respectively, where $p_0 < p^* < p_i$ and $T^*(p_i) < T^*(p^*) < T^*(p_0)$.

Referring to a physical system as shown in Fig. 1, the steady-state one-dimensional (in r) thermal energy equations for solid and fluid, respectively, are [11]:

$$(1-\varepsilon)\frac{1}{r^n}\frac{d}{dr}\left(k_s r^n \frac{dT_s}{dr}\right) - h_v(T_s - T_f) + q = 0 \tag{3a}$$

$$\varepsilon\frac{1}{r^n}\frac{d}{dr}\left(k_f r^n \frac{dT_f}{dr}\right) + h_v(T_s - T_f) - C_{pf}\rho_f v_r \varepsilon \frac{dT_f}{dr} = 0. \tag{3b}$$

Here, s and f refer to solid and fluid, respectively, h_v is the average volumetric heat transfer coefficient between the solid and fluid phases and ε is the porosity of the matrix.

We now define the following dimensionless variables:

$$R = r/(r_0 - r_i) \quad P = (p - p_0)/(p_i - p_0) \quad \theta = (T - T_i)/(T_0 - T_i) \tag{4}$$

$$\bar{v} = -\frac{\kappa}{\mu_l}\frac{p_i - p_0}{r_i - r_0} \quad V_r = \frac{v_r}{\bar{v}} \quad Re = \frac{\bar{v}}{\nu_l}\frac{b_g}{a_g}$$

$$A = \frac{a}{a_g}\frac{v_f}{v_l} \quad B = Re\frac{\rho_l}{\rho_f}\frac{b}{b_g} \quad \dot{M}_f = \frac{\dot{m}_f}{\rho_l \bar{v}(r_0 - r_i)^n}$$

$$D_f = \frac{C_{pf}\dot{m}_f(r_0 - r_i)^{1-n}}{(2\pi)^n k_f \varepsilon} \quad N = \frac{q(r_0 - r_i)^2}{(T_0 - T_i)k_s(1-\varepsilon)} \quad Q_r = \frac{q_r(r_0 - r_i)}{(T_0 - T_i)k_f\varepsilon}$$

$$Nu_s = \frac{h_v(r_0 - r_i)^2}{k_s(1-\varepsilon)} \quad Nu_f = \frac{h_v(r_0 - r_i)^2}{k_f\varepsilon} \quad Nu_{s,f} = \frac{Nu_s}{Nu_f}$$

$$Ja = \frac{\lambda\rho_v}{C_{pl}\rho_l(T_0 - T_i)} \quad K_{s,f} = \frac{k_s(1-\varepsilon)}{k_f\varepsilon}$$

$$\rho_{l,v} = \rho_l/\rho_v \quad \nu_{l,v} = \nu_l/\nu_v \quad C_{pl,v} = C_{pl}/C_{pv}$$

where the subscripts l, v refer to liquid and vapor, respectively. With reference to the above definitions, the continuity, motion and energy equations are transformed to the following dimensionless forms:

$$\frac{\mathrm{d}}{\mathrm{d}R}(V_r R^n) = 0 \tag{5}$$

$$-\frac{\mathrm{d}P}{\mathrm{d}R} = A\dot{M}_f/(2\pi R)^n + B\dot{M}_f/(2\pi R)^{2n} \tag{6}$$

$$\frac{\mathrm{d}^2\theta_s}{\mathrm{d}R^2} + \frac{n}{R}\frac{\mathrm{d}\theta_s}{\mathrm{d}R} - Nu_s(\theta_s - \theta_f) + N = 0 \tag{7a}$$

$$\frac{\mathrm{d}^2\theta_f}{\mathrm{d}R^2} + \frac{nR^{n-1} - D_f}{R^n}\frac{\mathrm{d}\theta_f}{\mathrm{d}R} + Nu_f(\theta_s - \theta_f) = 0. \tag{7b}$$

The boundary conditions applicable to this problem are:

$$R = R_i \quad P = 1 \quad \theta = \theta_w \tag{8a}$$

$$R = R_b \quad P = P_b \quad \theta = \theta_b \tag{8b}$$

$$R = R_c \quad P = P_c^* \quad \theta = \theta_c^* \tag{8c}$$

$$R = R_d \quad P = P_d^* \quad \theta = \theta_d^* \tag{8d}$$

$$R = R_0 \quad P = 0 \quad \theta = \theta_0 \tag{8e}$$

where $R_b - R_i$ is the dimensionless dispenser width and R_c and R_d are the dimensionless phase-change "interfaces" position (see Fig. 1)—to be determined. Note that R_b, θ_b, R_c, R_d and θ_d^* are not *a priori* known. θ_c^* is prescribed as a normal boiling point.

(C) PROCEDURE OF SOLUTION: PLANE CONFIGURATION, $n = 0$

The pressure distributions and temperature profiles are now obtained by solving the momentum and energy equations for each region. Also, the mass flow rate is obtained by utilizing the pressure profiles for evaluating pressure gradient. The solutions proceed here for a plane configuration, $n = 0$. The cylindrical shape is treated in part II of the publication [12].

(C)1. *Solution for the pressure distribution*

Combining the equation of continuity with the equation of motion, equations (5) and (6), respectively and integrating in the appropriate pressure limits for each domain, equation (8), yields the pressure distribution in the dispenser region, liquid and vapor regions of the working element:

$$P_n = P_i - (A_n\dot{M}_n + B_n\dot{M}_n^2)R \tag{9a}$$

$$P_l = P_b - (A_l\dot{M}_l + B_l\dot{M}_l^2)(R - R_b) \tag{9b}$$

$$P_v = P_d^* - (A_v\dot{M}_v + B_v\dot{M}_v^2)(R - R_d) \tag{9c}$$

where the subscripts n, l and v refer to the dispenser domain, liquid and vapour region, respectively.

Differentiating equation (9) and introducing the pressure gradient in the equation of motion, equation (6) yields relationships between the mass flow rate and the pressure limits in each region:

$$P_b = P_i - (A_n\dot{M}_n + B_n\dot{M}_n^2)R_b \tag{10a}$$

$$P_c^* = P_b - (A_l\dot{M}_l + B_l\dot{M}_l^2)(R_c - R_b) \tag{10b}$$

$$P_0 = P_d^* - (A_v\dot{M}_v + B_v\dot{M}_v^2)(R_0 - R_d) \tag{10c}$$

Since a steady-state is considered here, the mass flow rate is the same over each region. Thus, $\dot{m}_n = \dot{m}_l = \dot{m}_v (\dot{M} = \dot{M}_n = \dot{M}_l = \dot{M}_v)$ and equation (10) yield:

$$[A_nR_b + A_l(R_c - R_b)]\dot{M} + [B_nR_b + B_l(R_c - R_b)]\dot{M}^2 + P_c^* = 1 \tag{11a}$$

$$(A_v\dot{M} + B_v\dot{M}^2)(R_0 - R_d) + (P_0 - P_d^*) = 0. \tag{11b}$$

Note that, the values of P_b and P_d^* are unknown but may be related to the mass flow rate or vice-versa, depends on the given parameters and the calculation procedure (see below).

(C)2. *Solution for the temperature profiles*

The solution of the system of differential equations (7a) and (7b) is obtained by the elimination of either the solid temperature, θ_s or the fluid temperature, θ_f, leading to a single fourth-order differential equation for the remaining dependent variable.

Introducing $n = 0$ (for plane geometry) into equation (7b), solving for θ_s and differentiating, yield:

$$\theta_s = \frac{D_f\theta_f' - \theta_f''}{Nu_f} + \theta_f \tag{12a}$$

and

$$\theta_s'' = \frac{D_f\theta_f''' - \theta_f''''}{Nu_f} + \theta_f''. \tag{12b}$$

equations (7a) and (7b) are now combined to eliminate the difference $(\theta_s - \theta_f)$, giving:

$$\theta_f'' - D_f\theta_f' + Nu_{f,s}(\theta_s'' + N) = 0. \tag{13}$$

Equation (12b) is used to eliminate θ_s'' in equation (13). The latter becomes:

$$\theta_f^{(4)} - D_f\theta_f^{(3)} - (Nu_f + Nu_s)\theta_f^{(2)} + D_f Nu_s\theta_f^{(1)} = Nu_f N \tag{14}$$

the solution of which is:

$$\theta_f = \frac{Nu_{f,s}N}{D_f}R + C_1\mathrm{e}^{\alpha R} + C_2\mathrm{e}^{\beta R} + C_3\mathrm{e}^{\gamma R} + C_0 \tag{15}$$

where α, β and γ are the roots of the cubic equation:

$$\frac{1}{Nu_s}\psi^3 - \frac{D_f}{Nu_s}\psi^2 - (1 + Nu_{f,s})\psi + D_f = 0. \tag{16}$$

The temperature distribution in the solid matrix is obtained by solving equation (7b) for $(\theta_s - \theta_f)$:

$$\theta_s - \theta_f = \frac{D_f\theta_f' - \theta_f''}{Nu_f}. \tag{17}$$

Differentiating equation (15) and substituting θ_f' and θ_f'' into equation (17) the local solid fluid temperature difference is obtained:

$$\theta_s - \theta_f = \frac{1}{Nu_f}Nu_{f,s}N + C_1\alpha(D_f - \alpha)\mathrm{e}^{\alpha R} + C_2\beta(D_f - \beta)\mathrm{e}^{\beta R} + C_3\gamma(D_f - \gamma)\mathrm{e}^{\gamma R}] \tag{18}$$

Due to the high value of the volumetric heat transfer coefficient $[\alpha(1/D_p)]$, the value of Nu_s is relatively large compared to the other parameters appearing in equation (16). Hence, two roots of equation (16) are large in comparison to the third, in which case, the root with the lowest value characterizes the temperature distribution while the others decay faster.

Consequently equations (15) and (18) reduce to

$$\theta_f = \frac{Nu_{f,s}N}{D_f}R + C_1 e^{\alpha R} + C_0 \tag{19}$$

$$\theta_s - \theta_f = \frac{1}{Nu_f}[Nu_{f,s}N + C_1\alpha(D_f-\alpha)e^{\alpha R}]. \tag{20}$$

The total heat flux at any surface is given by:

$$q_r = -k_s(1-\varepsilon)\frac{dT_s}{dr} - k_f\varepsilon\frac{dT_f}{dr}. \tag{21}$$

Differentiating equations (19) and (20) and introducing the temperature gradient in the solid and fluid phase into equation (21) dimensionless form of the latter is:

$$|Q_r| = (K_{s,l}+K_{f,l})\frac{Nu_{f,s}N}{D_f} + \left[K_{s,l}+K_{f,l}+\frac{K_{s,l}}{Nu_f}\alpha(D_f-\alpha)\right]\alpha C_1 e^{\alpha R} \tag{22}$$

where $K_{s,l}$ and $K_{f,l}$ are $k_s(1-\varepsilon)/(\varepsilon k_l)$ and k_f/k_l, respectively. Hence, $K_{f,l}$ reduce to 1 in all liquid regions or to k_v/k_l in the vapour region.

Equations (19), (20) and (22) are valid for each section of the working element. For the dispenser section these equations simply reduce to:

$$\theta_f = C_1 e^{\alpha R} + C_0 \tag{23}$$

$$\theta_s - \theta_f = [C_1\alpha(D_f-\alpha)e^{\alpha R}]/Nu_f \tag{24}$$

and

$$|Q_r| = \left[K_{s,l}+K_{f,l}+\frac{K_{s,l}}{Nu_f}\alpha(D_f-\alpha)\right]\alpha C_1 e^{\alpha R} \tag{25}$$

since no internal heat is generated within the dispenser.

(C)3. *Temperature profile at entry region*

The energy equation and boundary conditions for the entry region are:

$$k_l\frac{d^2T_l}{dr^2} - \dot{m}_l C_{pl}\frac{dT_l}{dr} = 0 \tag{26a}$$

$$T = T_i \quad \text{at} \quad r \to -\infty \tag{26b}$$

$$T = T_w \quad \text{at} \quad r \to 0 \tag{26c}$$

where T_i is the approach temperature of the liquid feed and T_w is the temperature at the rear surface of the dispenser. The solution of equation (26) and the heat flux at $R = R_i$ in dimensionless form are:

$$\theta_l = \theta_w \exp(D_l R) \tag{26d}$$

$$|Q_i| = D_l\theta_w \tag{26e}$$

$$D_l = \dot{m}_l C_{pl}(r_0 - r_i)/k_l. \tag{26f}$$

(C)4. *Temperature profile in the evaporation region*

The solution for the solid and fluid temperature in the evaporation region may be simplified by assuming that the phase-conversion of fluid in this region proceeds at constant temperature. Though a pressure gradient does exist through this section, the corresponding saturation temperature varies only slightly for many fluids. As an example, for water flowing through a bed of packed sand of length up to 1 m the pressure drop is about 10^3 N/m^2 and the corresponding variation in the saturation temperature of water (around a pressure of one atmosphere) is less than 2°C.

Assuming $\theta_f \approx$ constant in this region equation (7a) may be rearranged in the form:

$$\frac{d^2(\theta_s-\theta_f)}{dR^2} - Nu_f(\theta_s-\theta_f) + N = 0 \tag{27}$$

the solution of which is:

$$\theta_s - \theta_f = \frac{1}{Nu_f}\{N + C_1\exp[(Nu_s)^{1/2}(R-R_c)] + C_2\exp[(Nu_s)^{1/2}(R-R_c)]\} \tag{27a}$$

where θ_f for this section is the average saturation temperature at R_c and R_d corresponding pressure P_c^* and P_d^*, respectively.

(D) CALCULATION PROCEDURE

The calculations of pressure and temperature distributions require the evaluation of the various constants of integration in each region. These are determined by combining the pressure and temperature boundary-conditions with the energy-balances which are applied on each section of the element. The derivation of all constants and relationships between the characteristic parameters is rather lengthy and thus, only typical expressions are brought here. Applying the boundary conditions at $R = R_i$ and $R = R_b$ while matching the heat flux at both sides of R_i and R_b yields two relationships between R_b, θ_w, Q_b as follows:

$$\frac{\theta_b}{\theta_w} = \exp(\alpha R_b) \tag{28a}$$

$$|Q_b| = D_l\theta_b. \tag{28b}$$

Similarly, the thermal conditions at the boundaries of the liquid region and a corresponding heat balance over R_b to R_c yield:

$$R_c - R_b = \frac{D_l\theta_c^*}{N K_{s,l}} \tag{29a}$$

$$\theta_b = (K_{s,l}+1.0)\frac{N K_{s,l}}{D_l^2} \times \{1.0 - \exp[-\alpha(R_c-R_b)]\}. \tag{29b}$$

Assuming a thermodynamic equilibrium in the two-phase region the pressure P_c^* at $R = R_c$ is the saturation vapor pressure corresponding to $\theta = \theta_c^*$. Since θ_c^* is prescribed P_c^* can be evaluated independently. The pressure P_b is calculated by equation

(10b), utilizing P_c^* and $(R_c - R_b)$ from equation (29a), and is in turn used in equation (10a) to calculate R_b.

For the superheating region, an energy balance reads:

$$D_v(\theta_0 - \theta_d^*) = N(R_0 - R_d)K_s, \qquad (30a)$$

where the corresponding saturation vapor pressure at $R - R_d$ is given by equation (11b). The corresponding saturation vapor pressure expression with equation (30a) and (11b) are solved for θ_d^* and R_d.

Also, the overall energy balance is

$$\theta_c^* + \frac{\theta_0 - \theta_d^*}{C_{pl,v}} + \rho_{l,v} Ja = \frac{N}{D_l} K_{s,l}(R_0 - R_b). \qquad (30b)$$

Introducing the computed values for θ_d^* and R_b in equation (30b) yields a new value for N. The average of the new and preceding values of N is used for subsequent calculations of the four regimes to evaluate a new N. The iterations are repeated until convergence is achieved. The calculation procedure is demonstrated in a flow chart in Appendix A of [13].

Note that the local volumetric heat-transfer coefficients in the various regimes of phases are evaluated by Littman and Sliva correlations [14].

(E) CALCULATED RESULTS AND DISCUSSION

Given the standard design data (P_i, P_0, T_i, T_c^*) and based on fluid and matrix structive properties, the deisgner usually wishes to predict the rate of internal heat generation which is required to yield a superheated fluid at a temperature level, T_0. The calculated results are presented below as a function of the downstream conditions at the exit ($R = R_0$) for various overall temperature drops through the element ($\Delta T_t = T_0 - T_i$).

The overall temperature variation through the element is represented by the Jacob number, Ja ($= \lambda \rho_v / C_{pl} \rho_l \Delta T_t$). Low value of Ja number indicates either high degree of superheat at the leading surface downstream, or highly subcooled liquid at the rear surface upstream. Similarly, high Ja number indicates that the outlet or inlet temperature are close to the saturation conditions.

Also are presented the dimensionless form of the basic variables, R_b, R_c and R_d, which, when combined with $\dot{M}$ and N, yield the pressure and temperature distributions through the reactor.

Figures 2, 3 represent the positions of the two phase-conversion interfaces, R_c and R_d, as a function of the superheat for various values of mass flux $\dot{M}$ and at different Jacob numbers, Ja. Also included in the figures are the corresponding thickness of the dispenser-layer, R_b. In general as $\theta_0 \to 0$ (or $\theta_i \to -1$) the outcoming vapour is at saturation condition, T_c^* and hence $R_d \to R_0$, and the main effect of the mass flux is on R_c and R_b, while R_d is unaffected either by $\dot{M}$ or by θ_0. On the other hand, as $\theta_0 \to 1.0$ (or $\theta_1 \to 0$) the incoming liquid is at the saturation temperature, and

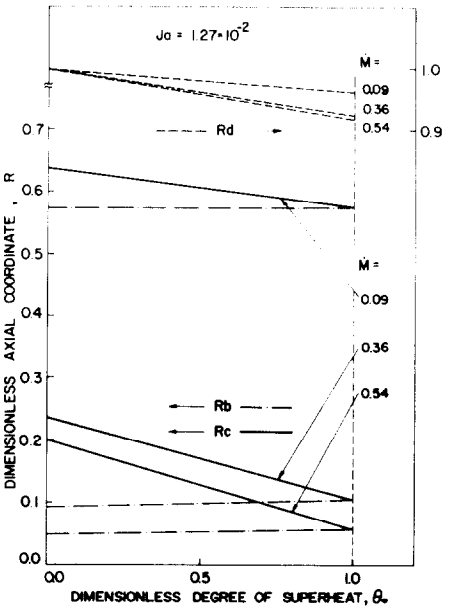

FIG. 2. Effect of mass flow rate on the position of phase-change interfaces for various degrees of superheat at $Ja = 1.27 \times 10^{-2}$.

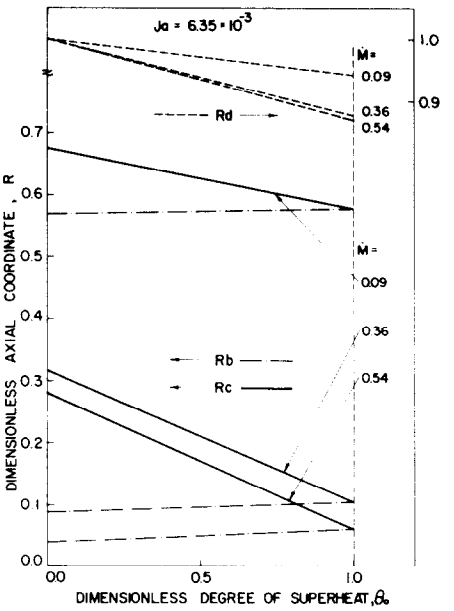

FIG. 3. Effect of mass flow rate on the position of phase-change "interfaces" for various degrees of superheat at $Ja = 6.35 \times 10^{-3}$.

hence $R_c \to R_b$. Thus, for higher superheat, the mass flux affects all R_b, R_c and R_d.

This effect is more pronounced for low mass flux for which the inertial contribution is neglected and hence the pressure gradient is lower in liquid phase (see Fig. 9). For high mass flux the dependence of the inertial resistance is of a velocity squared and hence its contribution is significant and the pressure gradient is higher for the same pressure drop, $1 - p_c^*$.

The effect of the Jacob number on the stratification of the various region (R_b, R_c and R_d) can be

evaluated by comparing Figs 2 and 3 for the different values of $\dot{M}$. For convenient comparison, this is demonstrated in Fig. 4 for one value of the mass flux. As is indicated in the figure, the effect of Jacob number on R_c or R_d is significant or not, depending upon whether low or high degrees of superheat are considered, respectively.

For a constant degree of superheat ($\theta_0 = \text{const.}$), an increase in Ja number (or a decrease in the overall temperature variation through the element, ΔT_t) yields a decrease in R_c while an increase in R_d. In other words, while the evaporation front at R_c moves inwardly upstream, the superheating front at R_d moves outwardly downstream. Thus, the evaporation region increases as the Jacob number increases.

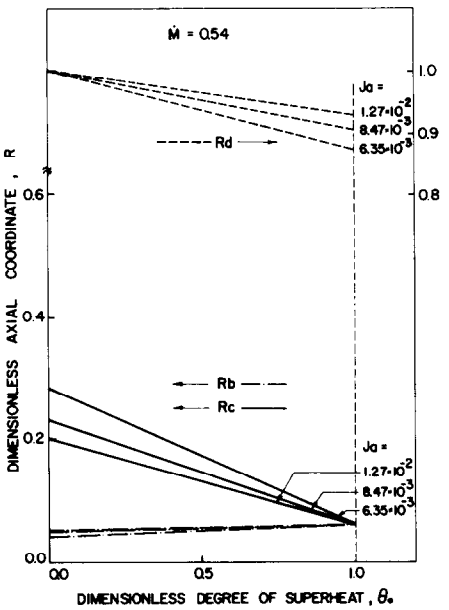

FIG. 4. Effect of Jacob number on the position of phase-change "interfaces" for various degrees of superheat for $\dot{M} = 0.54$.

Figures 2–4 also show that there is but a slight effect of the Jacob number and the level of superheat on the dispenser thickness, R_b. The value of R_b is mainly affected by the imposed mass flux through the element.

Figures 5 and 6 represent the required rate of internal heat generation as a function of the vapour superheat for various values of Jacob number. At constant Jacob number, high superheat means relatively high inlet temperature of liquid feed. In other words, as the superheat increases, the energy required to preheat the incoming liquid to saturation decreases, while this fraction of energy which is required to superheat the saturated vapour at R_d increases. However, since the heat capacity of the liquid phase is the larger, smaller preheating means smaller rates of heat generation. As is expected, this affect is more pronounced for higher mass flux, and a

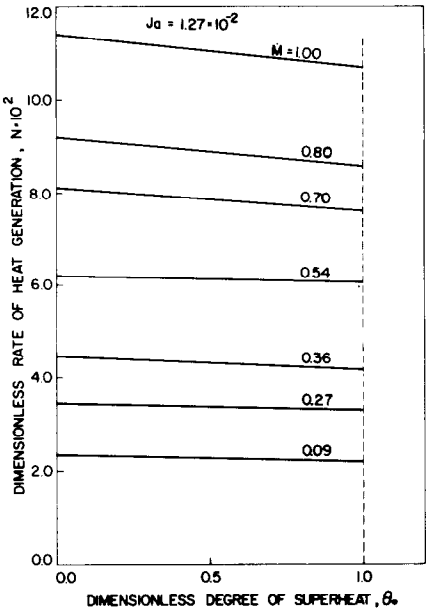

FIG. 5. Heat generation rate required for various mass flow rates at $Ja = 1.27 \times 10^{-2}$.

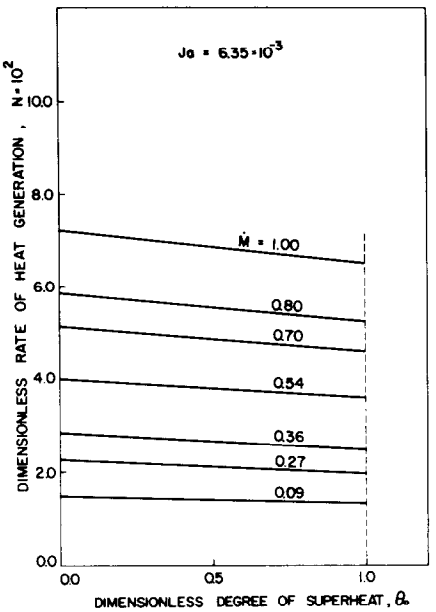

FIG. 6. Heat generation rate required for various mass flow rates at $Ja = 6.35 \times 10^{-3}$.

decrease of N with increasing θ_0 is noticed for the larger values of $\dot{M}$. Note also that in comparing Figs. 5 and 6, it should be kept in mind that both the dimensionless rate of heat generation and the Jacob number include the overall temperature drops through the element, ΔT_t. Thus, the value of N must be compared on a basis of constant ΔT_t or constant Ja.

Heat load N as a function of the mass flux $\dot{M}$ passes through a minimum which differs slightly for various Ja and θ_0, Fig. 7. In the region of positive gradient ($dN/d\dot{M}$), the increasing behaviour of N with increasing $\dot{M}$ is quite logical. In this regime of $\dot{M}$ values the inertial term in the pressure drop

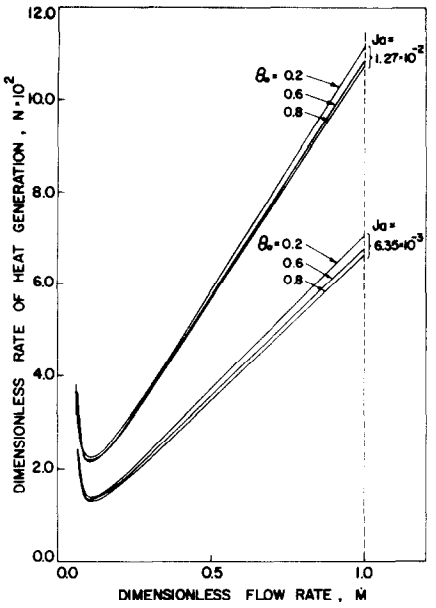

FIG. 7. Variation of internal heat generation with mass flow rate for various operation conditions.

expression in equation (1) is very significant and R_b, R_c, and R_d interfaces position change behaves quite uniformly (Figs. 2–4). As the mass flux decreases, the inertial term is neglected in relation to the viscous one and R_b, R_c and R_d interfaces position change is sharply pronounced. This causes the drastic decrease in the denominator term $(R_0 - R_b)$ and hence increasing N values for decreasing $\dot{M}$ in which the gradient is negative.

Figure 8 represents the temperature θ_b (at $R = R_b$) for various operation conditions. Sufficiently low temperature at the entry to the working section ($R = R_b$) is essential for stable operation of the reactor. However, it is well known that thermal conduction from the solid structure as well as from the liquid preheating region may bring about a subcooled boiling at the entry. Appearance of vapour bubbles may disturb the liquid feed penetration to the heated section, and the element being starved of coolant in the neighbourhood of boiling sites, would rise in temperature and thus burnout of the solid results. As is indicated in Fig. 8, the rise of the temperature at the entry due to thermal conduction must be considered, particularly at low flow rates.

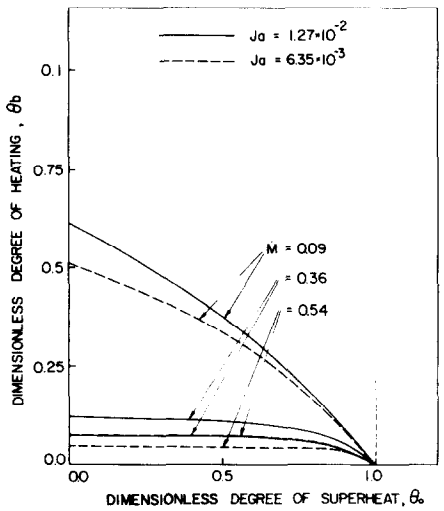

FIG. 8. Dispenser exit temperature for various operating conditions.

Figure 9 demonstrates the pressure distribution across the various regions. As is indicated in the figure, the major pressure drop occurs through the adjoining buffer dispenser due to its low permeability. Also, as is expected, the pressure drop across the superheating region is relatively small compared with that across the liquid preheating region.

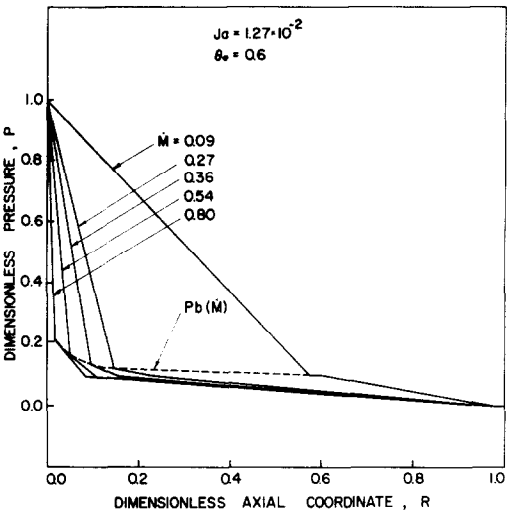

FIG. 9. Pressure distribution within the element for various mass flow rates at $Ja = 1.27 \times 10^{-2}$ and $\theta_0 = 0.6$.

The dimensionless temperature profiles in the various regions are shown in Fig. 10. Note that θ_l denotes the temperature variation in the dispenser or liquid regions, and θ_v denotes the temperature variation in the superheating region (both are defined with reference to T_i so that the dimensionless value at the outlet is always 1.0). The liquid is slightly heated in the dispenser region due to conduction but the main increase in the temperature occurs in the liquid and vapour regions. The intersection of the temperature profiles in these regions with the saturation line indicates the values of R_c and R_d, respectively.

F. FINAL REMARKS

The temperature profiles shown in Fig. 10 refer to the working fluid passing through the porous structure. The deviation of the temperature distribution within the solid matrix from the adjacent fluid is shown in Fig. 11. This deviation is lowest at the dispenser region where no internal heat is generated, and is highest at $R = R_b$, where internal heat generation commences and the entering fluid

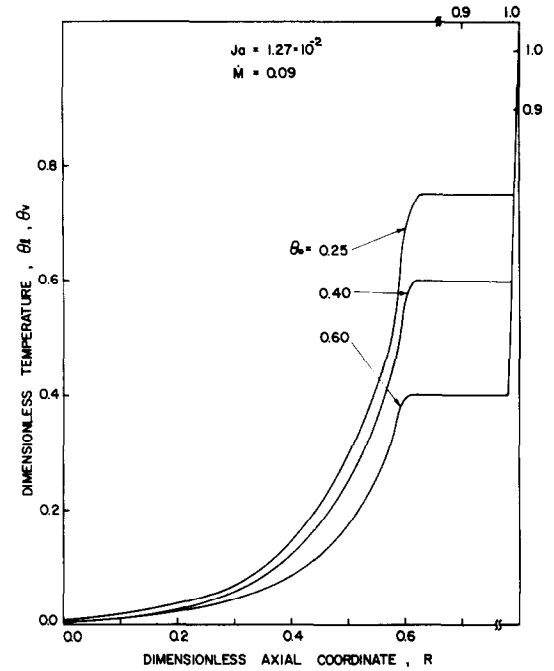

FIG. 10. Dimensionless temperature profiles θ_l, θ_v for various degrees of superheat at $Ja = 1.27 \times 10^{-2}$ and $\dot{M} = 0.09$.

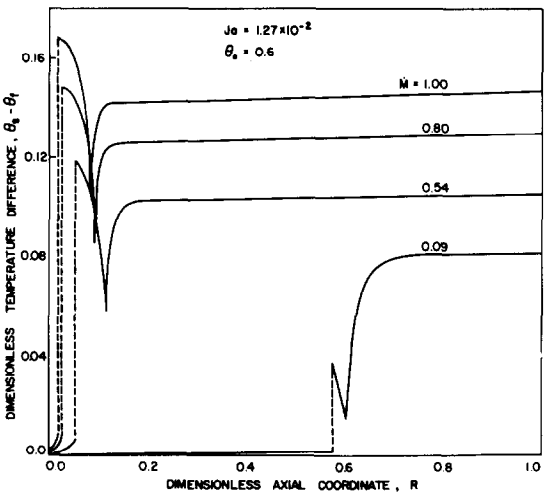

FIG. 11. Dimensionless temperature difference $\theta_s - \theta_f$ for various mass flow rates at $Ja = 1.27 \times 10^{-2}$ and $\theta_0 = 0.6$.

(which has been only slightly heated at previous region due to conduction) is still rather cold. At this point, as liquid is being rapidly heated (see Fig. 10) the solid–fluid temperature difference drops until evaporation starts and consequently a saturated liquid–vapour mixture is obtained.

At the junction of the buffer layer to the porous element, R_b, there is a discontinuity in solid temperature, θ_s (while the liquid temperature, θ_l is continuous here) because of change in solid thermal conductivity and the heat generation within one of the layers.

In general it is interesting to note that solid–fluid temperature difference is relatively small through all regions of the porous reactor. This theoretical result is consistent with the experimental measurements reported by Wong and Dybbs [5]. Consequently, one may comfortably speculate that the assumption of continuum which has been made under the conditions of slow flow through the porous medium is sufficiently reasonable for non-Darcy flow regimes. In other words, average or "macroscopic" energy equation can be applied for the heterogeneous solid–fluid system. It is, however, necessary to use effective properties of the saturated porous medium. This is highly rewarding in view of the complexity associated with a separated treatment of solid and fluid compared to the analysis of a continuum.

In this physical model the operation characteristics in the element as: R_b, R_c, R_d, θ_d^*, and N are not functions of heat-transfer coefficient. The latter affects the value of θ_b, temperature profiles, θ_l, θ_v, and the temperature difference profile, $\theta_s - \theta_l$, $\theta_s - \theta_v$.

REFERENCES

1. D. Moalem Maron, Steady state heat transfer within porous medium with temperature dependent heat generation, *Int. J. Heat Mass Transfer* **19,** 529 (1976).
2. D. Moalem Maron, General analysis of porous reactors with temperature-dependent rate of heat generation; plane, cylindrical and spherical elements, *Proceedings of the Sixth International Conference on Heat and Mass Transfer*, 7–11 August 1978, Toronto, Canada.
3. D. Moalem Maron and S. Cohen, Theoretical analysis of steady and transient operation of internally energised porous element under phase conversion and vapour superheat, *Int. J. Heat Mass Transfer* **19,** 1415 (1976).
4. L. Green, Gas cooling of porous heat source, *J. Appl. Mech.* **19**(2) 173 (1952).
5. K. F. Wong and A. Dybbs, An experimental study of thermal equilibrium in liquid saturated porous media, *Int. J. Heat Mass Transfer* **19,** 234 (1976).
6. G. S. Beavers and E. M. Sparrow, Non-Darcy flow through fibrous porous media, *J. Appl. Mech.* **36**(4), 711 (1969).
7. J. R. Schuster and T. G. Lee, Application of an improved transpiration cooling concept to space shuttle type vehicles, *J. Spacecraft* **9,** 804 (1972).
8. J. C. Koh and E. P. Del Casal, Two-phase flows in porous matrices for transpiration cooling, in *Developments in Mechanics*, Edited by J. E. Cermak and J. R. Goodman. Colorado State University (1968).
9. L. Green and P. Duwez, Fluid flow through porous metals, *J. Appl. Mech.* **73,** 39 (1951).
10. A. V. Luikov, L. L. Vasiliev and V. A. Mayorov, Static characteristics of equilibrium two-phase transpiration cooling system, *Int. J. Heat Mass Transfer* **18,** 863 (1975).
11. D. W. Green, R. H. Perry and R. E. Babcock, Longitudinal dispersion of thermal energy through porous media with a flowing fluid, *A.I.Ch.E. Jl.* **10,** 645 (1964).
12. S. Cohen and D. Moalem Maron, Non-Darcy flow with change of phase in internally energised cylindrical shaped porous element, *Israel J. Technol.* **15,** 356 (1977).
13. S. Cohen, Development of porous reactor, heat transfer in porous media with phase change, M.Sc. Thesis, Tel-Aviv University, Tel-Aviv, (1977).
14. H. Littman and Daniel E. Silva, Gas-particle heat transfer coefficients in packed beds at low Reynolds numbers, *Proceedings of the 4th International Heat Transfer Conference*, Paris-Versailles, Paper CT 1.4 (1970).

ECOULEMENT AVEC CHANGEMENT DE PHASE DANS UNE PLAQUE POREUSE

Résumé—On présente une étude théorique de l'écoulement d'un fluide avec conversion de phase et vapeur surchauffée dans un milieu poreux chauffé de façon interne. On considère un régime d'écoulement ne suivant pas la loi de Darcy. Les distributions de température dans le solide et les phases du fluide sont déterminées simultanément et on trouve que la différence entre eux, dans l'opération stationnaire, est relativement faible. Pour des conditions opératoirse variées, des paramètres caractéristiques sont évalués et calculés en incluant la densité de chaleur interne créée et nécessaire.

ТЕЧЕНИЕ С ФАЗОВЫМ ПЕРЕХОДОМ В ПЛОСКОМ ПОРИСТОМ ЭЛЕМЕНТЕ С ВНУТРЕННИМ ТЕПЛОВЫДЕЛЕНИЕМ, НЕ ПОДЧИНЯЮЩЕЕСЯ ЗАКОНУ ДАРСИ

Аннотация — Представлен теоретический анализ течения жидкости через пористый материал с внутренним источником тепла при наличии фазового перехода и перегрева пара. Рассматривается режим течения, не подчиняющийся закону Дарси. В результате расчёта распределений температуры в твёрдом теле и жидкости найдено, что в стационарных условиях различие между ними относительно невелико. Проведены оценка и расчёт характеристических параметров, включая интенсивность внутреннего тепловыделения, для различных рабочих условий.

NICHT-DARCY'SCHE STRÖMUNG MIT PHASENÄNDERUNG IN EINEM FLACHEN PORÖSEN ELEMENT MIT INNERER ENERGIEZUFUHR

Zusammenfassung—Es wird von einer theoretischen Studie über die Flüssigkeitsströmung durch ein von innen beheiztes poröses Medium, bei dem Phasenänderung und Überhitzung des Dampfes auftritt, berichtet. Dabei wird der nicht-Darcy'sche Strömungszustand betrachtet. Die Temperaturverteilungen in der festen und der flüssigen Phase werden simultan bestimmt, wobei sich zeigt, daß der Unterschied zwischen beiden unter stationären Bedingungen verhältnismäßig klein ist. Die für verschiedene Betriebsbedingungen charakteristischen Parameter einschließlich der erforderlichen inneren Wärmeerzeugung werden ermittelt und ihre Werte berechnet.